Pergamon

Int. J. Heat Mass Transfer. Vol. 40, No. 12, pp. 2859–2868, 1997
© 1997 Elsevier Science Ltd. All rights reserved
Printed in Great Britain
0017-9310/97 $17.00+0.00

PII: S0017-9310(96)00329-8

Towards a general numerical scheme for solidification systems

C. R. SWAMINATHAN✠ and V. R. VOLLER†

Saint Anthony Falls Laboratory, Department of Civil Engineering, University of Minnesota, Minneapolis, MN 55455, U.S.A.

(*Received* 19 *July* 1996 *and in final form* 13 *September* 1996)

Abstract—A central problem in the numerical treatment of the solidification of alloys is the coupling between the temperature and concentration fields. In this paper, governing equations and relationships that describe the temperature–solute coupling in a multicomponent alloy are presented. An overview of previous numerical coupling schemes is outlined. Following the presentation of a mixed explicit/implicit discretization of the governing equations a new numerical temperature–solute coupling scheme is developed. This new scheme can model the solidification of multicomponent alloys for a wide range of local scale behaviors. The performance of the scheme is tested on comparing numerical predictions for a ternary eutectic alloy with results obtained from a similarity solution. © 1997 Elsevier Science Ltd.

1. INTRODUCTION

The solidification of a multicomponent system is characterized, at the macroscopic scale, by a solid + liquid mushy region. Within this region the relationship between the temperature and solutal concentrations is controlled by the phase thermodynamics and local scale, microscopic transport processes. Numerical modeling involves the calculation of nodal temperature and concentration fields that simultaneously satisfy the macro scale transport equations and, in the mushy region, meet the constraints imposed by the thermodynamics and local scale processes. In the recent literature, a number of workers [1–17] provided accounts of how this temperature–solutal coupling can be achieved. For the most part, however, the schemes presented:

(1) Are only applied to binary systems [1–16], the recent work on modeling the solidification of steel reported by Schneider and Beckermann [17] being one exception.
(2) Impose limiting treatments of the local scale behavior, e.g. the lever rule [1–4, 13–16], requiring the assumption of complete solutal mixing in both the solid and liquid phases.

The objective of this paper is to review some of the previous temperature–solutal coupling schemes and to present a new scheme which has a high degree of generality. In particular the new scheme:

(1) Can be applied to a wide range of solidification systems, from pure material through to multicomponent alloy systems.
(2) Can readily incorporate general treatments of the local scale behavior.

2. GOVERNING EQUATIONS

2.1. *Assumptions*

Governing equations for the solidification of a multicomponent system are derived on additively combining the two phase volume averaged equations presented by Ni and Beckermann [18]. In carrying out this step five, basic assumptions valid across a very wide number of systems, are employed.

(1) The solid phase is fixed, i.e. the morphology of the mushy region is columnar dendritic or consolidated equiaxed.
(2) Within a representative elementary volume (REV) of the mushy region (order of 10^{-2}–10^{-3} m [18]) the temperature is uniform.
(3) Within the liquid fraction of the REV solutal concentrations are uniform; a realistic case for many alloys [19].
(4) Thermodynamic equilibrium holds at the solid–liquid interface, i.e. for each constituent species

$$C_s^I = kC_l \tag{1}$$

where k is the partition coefficient, the subscripts s and l refer to the solid and liquid phases, respectively, and the superscript $[]^I$ indicates evaluation at the solid–liquid interface. Equation (1) taken with assumptions 2 and 3 implies that the temperature and the liquid solute concentrations in an REV lie on the liquidus surface of the phase diagram.

✠ Deceased. Formerly with Creare Inc., Etna Road, P.O. Box 71, Hanover, NH 03755, U.S.A.
† Author to whom correspondence should be addressed.

NOMENCLATURE

a	numerical coefficient
c	specific heat capacity
C	concentration
$\langle C_s \rangle^s$	intrinsic volume average of solute concentration in solid phase
g	liquid volume fraction
h	enthalpy
K	thermal conductivity
k	partition coefficient
m	slope of the liquidus line
S	source term
t	time
T	temperature
$\mathbf{u}$	volume flux of interdentritic fluid.

Greek symbols

α	Fourier diffusion number
β	microsegregation parameter
γ	microsegregation parameter
ΔH	latent heat
Δt	simulation time step
$[\rho C]$	mixture solute density
$[\rho H]$	mixture volumetric enthalpy
ρ	density
ϕ	general dependent variable.

Subscript

eut	eutectic
l	liquid
N	total number of species
nb	neighbor nodes of P
P	node point P
s	solid.

Superscript

aux	auxiliary value
equ	equilibrium value
I	interface quantity
n	iteration level
old	old time step.

(5) At the macroscopic scale of a solidification process (order of meters) solutal mass diffusion is negligible.

2.2. *Basic equations*

With these assumptions appropriate mixture equations for multicomponent solidification are as follows.
Energy conservation:

$$\frac{\partial}{\partial t}[\rho H] + \nabla \cdot (\rho_l \mathbf{u} h_l) = \nabla \cdot (K \nabla T). \tag{2}$$

Species conservation (one equation for each constituent species):

$$\frac{\partial}{\partial t}[\rho C] + \nabla \cdot (\rho_l \mathbf{u} C_l) = 0. \tag{3}$$

Mass conservation:

$$\frac{\partial}{\partial t}[\rho] + \nabla \cdot (\rho_l \mathbf{u}) = 0 \tag{4}$$

where $\mathbf{u}$ [m^3 m^{-2}-s^{-1}] is the volume flux of interdentritic fluid and K [J m^{-1} K^{-1}-s^{-1}] is the mixture conductivity, in its most general form a tensor dependent on the morphology in the solid/liquid REV and the conductivities in the solid and liquid phases. Equations (2)–(4) are sufficient to fully examine the coupling mechanism between the solute and thermal fields.

2.3. *Definition of mixture terms*

A full definition of the mixture terms in equations (2)–(4), denoted by the use of square brackets, is required. Appropriate definitions are:

Mixture density [kg m^{-3}]

$$[\rho] = (1-g)\rho_s + g\rho_l, \tag{5}$$

where g is the liquid volume fraction in the REV, and ρ_s and ρ_l are the solid and liquid intrinsic volume averaged densities, note fluctuating components have been neglected [18].
Mixture volumetric enthalpy [J m^{-3}]

$$[\rho H] = (1-g)\rho_s h_s + g\rho_l h_l. \tag{6}$$

After appropriate linearization the phase enthalpies [J kg^{-1}] can be defined as

$$h_s = c_s(T, \langle C_s^1 \rangle^s, \langle C_s^2 \rangle^s, \ldots, \langle C_s^N \rangle^s)T \tag{7}$$

and

$$h_l = c_l(T, C_l^1, C_l^2, \ldots C_l^N)T + \Delta H \tag{8}$$

where $\langle C_s^i \rangle^s$ is the intrinsic volume average of the ith species concentration in the solid and C_l^i is the ith species concentration in the liquid. The terms c_s and c_l are nominal specific heats and the term ΔH (a constant) is the latent heat of fusion at a reference temperature, without loss of generality a reference temperature of $T = 0$ is chosen. These definitions of the phase enthalpies are preferred because they can take full account of variations due to both temperature and phase concentrations, e.g. see the lead–tin system studied by Poirier and Nandapurkar [20].

Substitution of equations (6)–(8) into equation (2), along with use of mass conservation leads to the temperature-source based energy equation used in this work

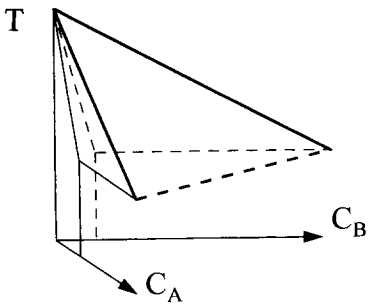

Fig. 1. Schematic of a section of the phase diagram of an example ternary alloy.

$$\frac{\partial}{\partial t}[\rho cT]+\nabla\cdot(\rho_l \mathbf{u} c_l T) = \nabla\cdot(K\nabla T)-\rho_s \Delta H\frac{\partial g}{\partial t} \quad (9)$$

where

$$[\rho c] = (1-g)\rho_s c_s + g\rho_l c_l. \quad (10)$$

Mixture solute density [kg m^{-3}]

For a given constituent species

$$[\rho C] = \rho_s(1-g)\langle C_s\rangle^s + g\rho_l C_l. \quad (11)$$

In the case of a uniform solid morphology in the REV this equation can be written as

$$[\rho C] = \rho_s\int_0^{1-g} C_s\,\mathrm{d}\Gamma + g\rho_l C_l. \quad (12)$$

2.4. *The phase diagram*

The temperature–solute coupling problem is closed on specifying the thermodynamics and the local scale transport behavior. The condition of thermodynamic equilibrium at the solid–liquid interface, equation (1), suggests that the liquidus surface in the phase diagram can be used to specify a relationship between the liquid concentrations and the temperature. In the most general form this relationship can be written as

$$T = G(C_l^1, C_l^2, \ldots, C_l^N). \quad (13)$$

In dilute systems, however, it is possible to approximate the liquidus surface as a summation of the slopes of liquidus lines [17]. For example in a ternary system ($N = 2$), assuming straight liquidus lines in the constituent binaries

$$T = T_f + m_l^1 C_l^1 + m_l^2 C_l^2 \quad (14)$$

where m_l^1 and m_l^2 are the liquidus slopes and T_f is the fusion temperature of the pure solvent. Figure 1 shows a schematic section of this ternary diagram. In this system one of the constituent binaries exhibits a continuous series of solute solutions. The other two constituent binaries, illustrated by the "wedge" in the figure, are simple eutectics. The liquidus surface is indicated by the triangle in bold outline and the eutectic line by a heavy dashed line.

2.5. *Local scale modeling*

A central step in the coupling of the solute and temperature is the correct accounting of the local scale mass diffusion that occurs in the dendritic arm spaces. The requirement is to, on specification of the liquid fraction, g, and solute density, $[\rho C]$, obtain a value for the REV liquid concentration, C_l. The value of C_l is controlled by the diffusion of the solute in the solid phase, often referred to as "back diffusion". In the simple case of complete solute diffusion in the solid local thermodynamic equilibrium is achieved and the lever rule,

$$[\rho C] = \rho_s k(1-g)C_l + g\rho_l C_l \quad (15)$$

can be used to obtain C_l. In the general case, however, the back diffusion is finite and a more detailed treatment of the local scale transport process is required. As a starting point it is noted that the derivative of equation (12) with respect to time is

$$\frac{\partial[\rho C]}{\partial t} = \rho_s k C_l\frac{\partial(1-g)}{\partial t} + \frac{\partial(\rho_l g C_l)}{\partial t} + \rho_s\int_0^{(1-g)}\frac{\partial C_s}{\partial t}\mathrm{d}\Gamma. \quad (16)$$

The last term in equation (16) is the rate of the back diffusion of solute and its representation is the key to the local scale modeling. In this paper two ways of representing this term are presented.

In the first approach, assuming constant phase densities for convenience of presentation, the back diffusion term is represented as [21]

$$\rho_s\int_0^{(1-g)}\frac{\partial C_s}{\partial t}\mathrm{d}\Gamma = \beta\rho_s(1-g)\frac{\partial kC_l}{\partial t}. \quad (17)$$

The parameter $0 \leqslant \beta \leqslant 1$, in equation (17), allows for a back diffusion treatment that lies between the limits of zero back diffusion ($\beta = 0$, the Scheil assumption) and complete back diffusion ($\beta = 1$, the lever rule). Substitution in equation (16) with rearrangement arrives at

$$\frac{\partial[\rho C]}{\partial t} = \frac{\partial}{\partial t}[\rho_l g C_l + \beta\rho_s(1-g)kC_l] - (1-\beta)\rho_s kC_l\frac{\partial g}{\partial t}. \quad (18)$$

For a given REV (which could be a cell in a computational solution domain) a finite difference solution of equation (18) gives an explicit expression for the solute concentration in the liquid,

$$C_l = \frac{[\rho C]-[\rho C]^{old}+[\rho_l g^{old}+\beta\rho_s(1-g^{old})k]C_l^{old}}{\rho_l g+\beta\rho_s(1-g)k+(1-\beta)\rho_s k(g^{old}-g)} \quad (19)$$

where the superscript $[]^{old}$ refers to values at old time. On setting

$$\beta = 2\alpha[1-e^{-1/\alpha}]-e^{-1/2\alpha} \quad (20)$$

where α is the standard Fourier diffusion number, this

proposed back diffusion treatment is equivalent to using the Clyne and Kurz correction [21] of the well known Brody and Flemings [22] back diffusion model.

An alternative representation of the back diffusion in terms of well defined physical parameters is due to Wang and Beckermann [19]. These authors model the back diffusion term in equation (16) as

$$\rho_s \int_0^{1-g} \frac{\partial C_s}{\partial t} d\Gamma = \rho_s \gamma (k C_l - \langle C_s \rangle^s) \tag{21}$$

where γ is a physical parameter which can be directly related to the morphology in the REV and the solid state mass diffusion coefficient [17, 19]. Substitution of equation (21) into equation (16) followed by a finite difference solution in time leads to the expression

$$C_l = \frac{[\rho C] - [\rho C]^{old} + \rho_l g^{old} C_l^{old} + \dfrac{\Delta t \gamma}{1-g}[\rho c]}{\rho_l g + \rho_s k (g^{old} - g) + \dfrac{\Delta t \gamma}{1-g}(\rho_s k (1-g) + \rho_l g)} \tag{22}$$

where Δt is the simulation time step. The limiting case of zero diffusion in the solid phase (the Scheil assumption) can be obtained on setting $\gamma = 0$ and the limiting case of complete diffusion in the solid (the lever rule) can be obtained on letting $\gamma \to \infty$.

Both equations (19) and (24) can be written in the general form

$$C_l = F([\rho C], g, \text{old values}) \tag{23}$$

where, in a numerical solution, C_l would be the nodal value of the liquid concentration for a given constituent species.

3. AN OVERVIEW OF PREVIOUS COUPLING SCHEMES

Before the general numerical scheme of coupling the solutal and thermal fields, which is the central contribution of this paper, is presented, it is worthwhile to provide an overview of some of the existing coupling schemes that can be found in the literature. A standard approach is the so called source based scheme. In this approach suitable discrete forms (usually based on an implicit time integration) of the governing temperature, equation (9), and solutal, equation (3), transport equations are solved. Typically, in a given time step of the calculation, a two level iterative technique is used with the following basic steps:

(1) On a specified grid of node points, distributed throughout the domain, the current nodal temperature, T and mixture solute density, $[\rho C]$, fields are calculated.

(2) At each node point, P, in the domain an auxiliary enthalpy value is calculated,

$$H_P^{aux} = c T_P^{n+1} + g_P^n \Delta H \tag{24}$$

where the superscript $[]^{n+1}$ and $[]^n$ indicate the current and previous iterate values, respectively. The parameter c is a representative specific heat, its value does not have to be precise since the role of equation (26) is only to provide a reference point during subsequent adjustment of the temperature, liquid fraction and liquid concentration fields.

(3) An inner iteration is performed that adjusts the nodal temperature field, T^{n+1}, and solves for the current, $(n+1)$th, liquid fraction and liquid concentration fields. The objective of this inner iteration is to find nodal fields that simultaneously satisfy the constraint equations

$$H_P^{aux} = c T_P^* + g_P^* \Delta H \quad \text{(a)}$$

$$[C_l]_P^* = F([\rho C]_P, g_P^*) \quad \text{(b)}$$

$$T_P^* = G((C_l^1)_P^*, (C_l^2)_P^*, \ldots, (C_l^N)_P^*) \quad \text{(c)} \tag{25}$$

where the superscript $[]^*$ indicates values that will change in the inner-iteration. Equation (25b), applied for each constituent species, is the constraint imposed on the local transport behavior in the REV, see equation (23). Equation (25c) is the constraint imposed by the liquidus surface, see equation (13).

(4) After convergence of the inner-iteration, the starred values become the appropriate $(n+1)$th outer iterative values.

(5) In closing the outer iteration a convergence check is made and if required the above steps are repeated.

A key step in this coupling approach is the inner-iteration. In the simplest inner-iteration, Voller *et al.* [6], use a one pass method, with calculations in the following order:

- starting with the nth iterate of the liquid concentration fields, equation (25c) is solved for T_P^*;
- the nodal liquid fraction, g_P^*, is calculated from equation (25a);
- the nodal liquid concentrations, C_P^*, are calculated from equation (25b); and
- to conclude, equation (25a) is used once more to update the nodal temperature.

This approach is simple to apply but has two drawbacks, the calculation of the nodal liquid fraction often requires underrelaxation and, at the early states of the outer-iteration, the fields emerging from the inner-iteration will not be fully consistent. This last problem, which inhibits the convergence of the outer-iterations, is overcome by Flood *et al.* [8] who use an inner-iteration with successive substitution, continuing the calculations steps of the Voller *et al.* approach until convergence of equation (25). Simple successive substitution may not always work and sometime it is more appropriate to apply a Newton solver for equation (25), an approach that has been

used by Voller and Sundarraj [10] for the temperature–solute coupling following an explicit time integration of the governing conservation equations. In some cases, as demonstrated by Prakash and Voller [7], it is possible to reduce equation (25) to a single quadratic equation in the nodal liquid fraction g_P. Solution of this quadratic is followed by an update of the nodal liquid concentration, equation (25b), and the nodal temperature, equation (25c). Bennon and Incropera [4] also form and solve a quadratic in the nodal liquid fraction; these authors, however, solve the energy equation in terms of enthalpy as opposed to temperature. Another extension to the source based scheme, suggested by Zeng and Faghri [15, 16], is to introduce a linearization of the source terms in the energy equation. A scheme that introduces additional stability into the iterative solution.

The temperature–solute coupling proposed by Schneider and Beckermann [17] offers an alternative to the direct iterative solution of equation (25). In this approach in the mushy zone:

- the discrete equation representing the conservation of the liquid concentration is substituted into the phase diagram relationship, equation (25b);
- the resulting temperature relationship is used in the energy conservation equation i.e. equation (9);
- this results in a nonlinear equation in the nodal solid fraction $(1-g_P)$, which is solved by a Newton method;
- the concentration conservation equations are then solved and the nodal temperatures in the mushy zone are updated using equation (25c).

This scheme has been successfully applied in modeling the solidification of multicomponent steel alloys.

4. A GENERAL SCHEME

Previous source based schemes for coupling the thermal and solutal fields involve the inner solution of a set of nonlinear equations. In the general case, this inner solution will be complex and involve iteration. The aim of the work in this paper is to develop a robust and efficient temperature–solutal coupling scheme that avoids the need of an inner solution of the nonlinear equations, equation (25).

4.1. *The numerical discretization*

The basic principal in a numerical scheme based on a volume discretization of a grid of nodes is to arrive at a set of algebraic equations that relate the value of a dependent variable, ϕ, at a given node P to values at the neighboring nodes, nb, via the specification of appropriate coefficients, a_P etc. A typical equation will have the form

$$(a_P+S_P)\phi_P=\sum_{\mathrm{nb}}a_{\mathrm{nb}}\phi_{\mathrm{nb}}-S_{\mathrm{C}} \tag{26}$$

where the source term $S=S_{\mathrm{P}}\phi_{\mathrm{P}}+S_{\mathrm{C}}$. Equation (26) represents a general discretization and its form can accommodate schemes based on both control volume methods and Galerkin finite element methods. The general discrete forms of the governing equations are as follows.

Energy: a fully time implicit integration of equation (9) with mass lumping of the source and transient terms gives

$$a_P T_P^{n+1}=a_P^{\mathrm{old}}T_P^{\mathrm{old}}+\sum_{\mathrm{nb}}a_{\mathrm{nb}}T_{\mathrm{nb}}^{n+1}+\rho_{\mathrm{s}}\Delta H(g_P^{\mathrm{old}}-g_P^{n+1}) \tag{27}$$

where, in calculating the coefficients the most current available iterate values are used and an upwinding treatment has been used for the advective terms. Following Swaminathan and Voller [23] the current iterate of the liquid fraction can be approximated as

$$g^{n+1}=g^n+\frac{\mathrm{d}g}{\mathrm{d}T}[T^{n+1}-T^n] \tag{28}$$

which on substitution into equation (27) results in the iterative equation

$$\left[a_P+\rho_{\mathrm{s}}\Delta H\frac{\mathrm{d}g}{\mathrm{d}T}\right]T_P^{\mathrm{aux}}=a_P^{\mathrm{old}}T_P^{\mathrm{old}}+\rho_{\mathrm{s}}\Delta H\frac{\mathrm{d}g}{\mathrm{d}T}T_P^n+\sum_{\mathrm{nb}}a_{\mathrm{nb}}T_{\mathrm{nb}}^{\mathrm{aux}}+\rho_{\mathrm{s}}\Delta H(g_P^{\mathrm{old}}-g_P^n) \tag{29}$$

where the superscript $[]^{\mathrm{aux}}$ has replaced the superscript $[]^{n+1}$ to indicate that these variables will be treated as auxiliary variables.

Solute conservation: the solute conservation, equation (3), is discretized using a fully explicit time integration, i.e. for each species in turn,

$$([\rho C])_P=([\rho C])_P^{\mathrm{old}}+\sum_{\mathrm{nb}}a_{\mathrm{nb}}(C_{\mathrm{l}})_P^{\mathrm{old}}. \tag{30}$$

Since, under usual circumstances, the mixture solute density, $[\rho C]$, will change slowly the explicit time solution of equation (30) will impose no serious stability restrictions on the choice of time step. This critical observation introduces a great deal of simplicity into the temperature–solutal coupling. The use of a mixed explicit/implicit time integration is seen as one of the major contributions of the current work.

4.2. *The solutions steps*

Assuming a specified flow field, the solution and coupling of the temperature and solutal fields is achieved with the following iterative steps.

(1) In problems involving phase changes that occur at single fixed temperature, e.g. pure materials or materials with a eutectic reaction the temperature scale is translated so that $T_{\mathrm{eut}}=0$.
(2) Initial iterate values ($n=0$) are set to old time step values.
(3) Equation (30) is solved for the mixture solute density $[\rho C]$. Note due to the explicit time inte-

gration this equation only needs to be solved once per time step.

(4) Equation (29) is solved for the auxiliary nodal temperature, T^{aux}. This step requires the evaluation, at each node, of the liquid fraction temperature slope, dg/dT. An exact evaluation would involve the evaluation of the partial derivatives of g with respect to temperature and concentration [15, 16]. In this work, the simple but effective and efficient direct approximation

$$\frac{dg}{dT} = \begin{cases} \dfrac{g_P^n - g_P^{n-1}}{T_P^n - T_P^{n-1} + 10^{-6}}, & 0 < g_P^n < 1 \\ 0, & g_P^n = 1 \quad \text{or } g_P^n = 0 \end{cases} \tag{31}$$

is used. There are three features to note in this treatment, (i) outside of the phase change (determined by the nth iterate of the liquid fraction) the slope is set to zero; (ii) the slope is calculated in terms of the two proceeding iterate values; and (iii) in cases where the temperature remains constant across an iteration (indicating a pure material or an eutectic reaction) the slope is defaulted to a large value.

(5) From the T^{aux} field current values of the liquid fraction are obtained from equation (28)

$$g_P^{n+1} = g_P^n + \text{SLOPE}\,[T_P^{aux} - T_P^{equ}] \tag{32}$$

where

$$T^{equ} = G(C_l, C_l^2, \ldots, C_l^N) \tag{33}$$

see equation (13), or for the specific case of a dilute ternary alloy equation (14). Note that nth iterate values are used on the right-hand side of equation (33). The term SLOPE in equation (32) is evaluated as

$$\text{SLOPE} = \begin{cases} \dfrac{dg}{dT}, & 0 < g_P^n < 1 \\ \dfrac{c_l}{L}, & g_P^n = 1 \quad \text{or } g_P^n = 0. \end{cases} \tag{34}$$

If node P is undergoing the phase change the value of SLOPE is set to the liquid–temperature slope, dg/dT. If node P is outside of the mushy region, in order to allow for the initiation of the phase change within a time step, the value of SLOPE takes the default value of c_l/L. In use equation (34) is applied to every node followed by an under-shoot/over-shoot correction that constraints nodal liquid fractions to take values between 0 and 1.

(6) Nodal values of liquid concentration C_l are obtained using the local scale model, i.e.

$$(C_l)_P^{n+1} = F([\rho C]_P, g_P^{n+1}, \text{old values}) \tag{35}$$

specific models could be based on the Clyne and Kurz [21] back diffusion mode, equation (19) or the Wang and Beckermann [19] model, equation (22).

(7) In a eutectic system if the liquid concentration calculated from the previous step exceeds the eutectic value it is pegged back and set equal to this value.

(8) The penultimate step of the iteration cycle is the calculation of the nodal temperature,

$$T_P^{n+1} = \begin{cases} G((C_l^1)_P^{n+1}, \ldots, (C_l^n)_P^{n+1}), & 0 < g_P^n < 1 \\ T_P^*, & g_P^n = 0 \quad \text{or } g_P^n = 1. \end{cases} \tag{36}$$

This sets the nodal temperature to the equilibrium temperature, T^{equ}, if node P is in the mushy region or to the auxiliary value calculated in step 4 if node P is not changing phase.

(9) The last step in the iteration cycle is the updating of the thermal constants, coefficients and if required the velocity field, which in general cases will involve the coupled solution of continuity and momentum equations.

(10) In the iteration cycle steps 4 to 9 are repeated until convergence. In current implementations convergence in a time step is declared when the maximum change in the nodal liquid fraction values falls below 10^{-5}.

5. TESTING

In testing the main concerns will be the accuracy and efficiency of the proposed temperature–solute coupling scheme. The accuracy of the coupling scheme relates to its ability to accurately solve the governing equations and related constraints imposed by the thermodynamics and the local scale behavior. Accuracy will be tested on comparing the predictive performance of the scheme with a recently developed semi-analytical similarity solution, fully described in a companion paper [24]. Emphasis will be placed on how accurately the proposed algorithm can deal with problems that involve (i) a finite back diffusion in the solid; (ii) multicomponent alloys; and (iii) macrosegregation.

Previous work by the authors [23] in developing algorithms for solving phase change problems with well defined liquid–fraction temperature relationships (i.e. phase changes that do not require an explicit temperature–solutal coupling) has shown that the most efficient algorithms require on the order of 2–4 iterations per time step to converge. In terms of efficiency the proposed scheme, which needs to achieve a temperature–solutal coupling, will be considered a success if it can match this performance.

Table 1. Properties and conditions used in test problems

Property	Value	Unit
c	1000	J kg^{-1} K^{-1}
K	100	W m^{-1} K^{-1}
ΔH	4×10^5	J kg^{-1}
T_{eut}	821.2	K
T_f	921.2	K
T_i	905.2	K
T_{chill}	621.2	K
k	0.15	—
ρ_l	2400	kg m^{-3}
ρ_s	3120	kg m^{-3}
C_0	5.0	wt%
m	3.4	—
m_1	3.4	—
m_2	7.2	—
C_0^1	2.5	wt%
C_0^2	1.18	wt%

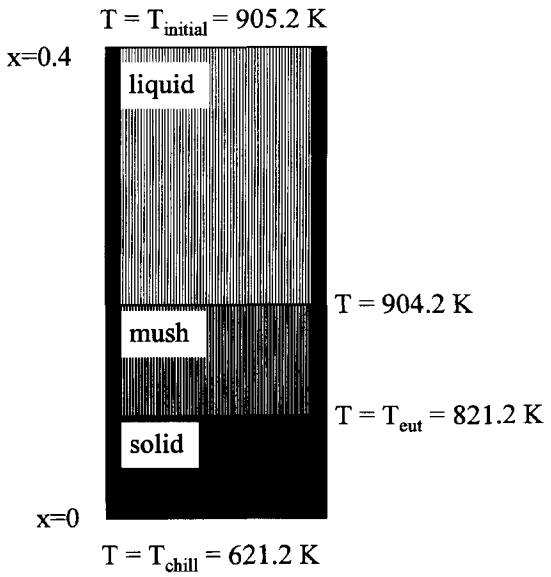

Fig. 2. Test geometry showing thermal boundary conditions.

5.1. *Test date and problem geometry*

In order to provide a match to real systems the data used is consistent with an Al–Cu system. There are some liberties taken, however. In particular: (i) to focus on temperature–solutal coupling issues constant thermal properties are assumed; (ii) in order to establish significant interdendritic fluid flow and hence macrosegregation a much larger than observed difference between the solid and liquid densities is imposed; and (iii) an artificial ternary system is used with constant liquidus slopes and an isothermal eutectic line, see Fig. 1. The appropriate data is given in Table 1. The proposed coupling scheme can deal with much more complex forms of the phase diagram, e.g. nonlinear slopes, nonconstant partition coefficients, etc. The choice of the test data in Table 1 is driven by the need to compare predictions with the similarity solution [24], a solution that needs a restricted definition of the phase diagram.

The test geometry involves the unidirectional solidification, from below, of the test alloy initially at a uniform composition and temperature. Figure 2 show a schematic of the test geometry and indicates the thermal boundary conditions. At any point in the process the test domain will consist of three regions, a fully solid region, a mushy region and a fully liquid region. Due to the difference in densities between the solid and liquid phases (see Table 1) there will be an interdendritic flow towards the chill face ($x = 0$) in the mushy zone. The resolution of this flow requires the solution of the flow field using a suitable discrete version of the mass continuity, equation (4). The interdendritic flow will establish a macrosegregation profile across the mushy region, i.e. the value of the mixture concentration, $[C] = [\rho C]/[\rho]$, will be a function of distance from the chill face. Accurate numerical predictions of the mixture concentration are the most difficult to obtain and as such the profiles of $[C](x)$ across the mushy region will be used throughout the testing of the proposed numerical scheme.

5.2. *Binary eutectic—lever model*

The first problem investigated is the solidification of a binary eutectic system. Figure 3 shows predicted $[C]$ profiles at times $t = 250$, 500 and 1000 s when local scale equilibrium (the lever rule) is assumed. In these calculations a grid of 400 equal spaced volumes in the domain $0 \leqslant x \leqslant 0.4$ is used with a simulation time step of $\Delta t = 1$ s. The predicted profiles are in very close agreement with those obtained using the similarity solution [24], indicated by the square symbols in Fig. 3. These results offer a clear indication that the proposed temperature–solutal coupling scheme accurately solves the model specified by the governing equations.

In carrying out the simulation to 1000 s an average of about 4 iterations per time step was needed to meet the given convergence criteria. This value is consistent with the performance of previous numerical schemes designed to solve macrosegregation free problems [23].

5.3. *Binary eutectic—general back diffusion*

A strength of the proposed numerical scheme is that it can deal with a range of local solid state diffusion behaviors. This feature is illustrated in Fig. 4 which shows the predicted concentration profiles in the mushy region at $t = 500$ s. In these predictions the Clyne and Kurz [21] model, equation (19), is used to model the back-diffusion in the solid. Three values of the β parameter are used, $\beta = 1$, corresponding to complete diffusion in the solid (the lever rule), $\beta = 0.5$ corresponding to a finite level of back-diffusion and $\beta = 0$ corresponding to zero back-diffusion (the Scheil approximation). These results indicate that (i) the level of back-diffusion does effect the concentration profiles in the mushy region; and (ii) numerical predictions from the proposed scheme when finite back-

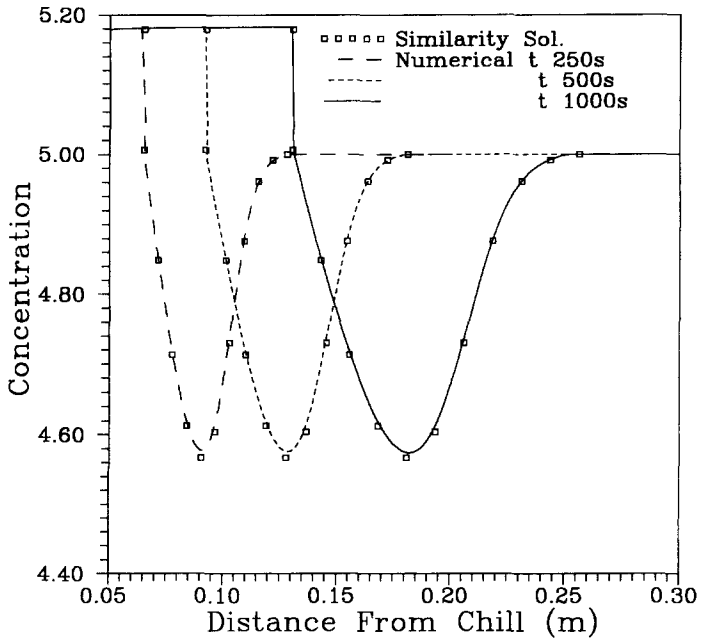

Fig. 3. Concentration profiles at times $t = 250$, 500 and 1000 s.

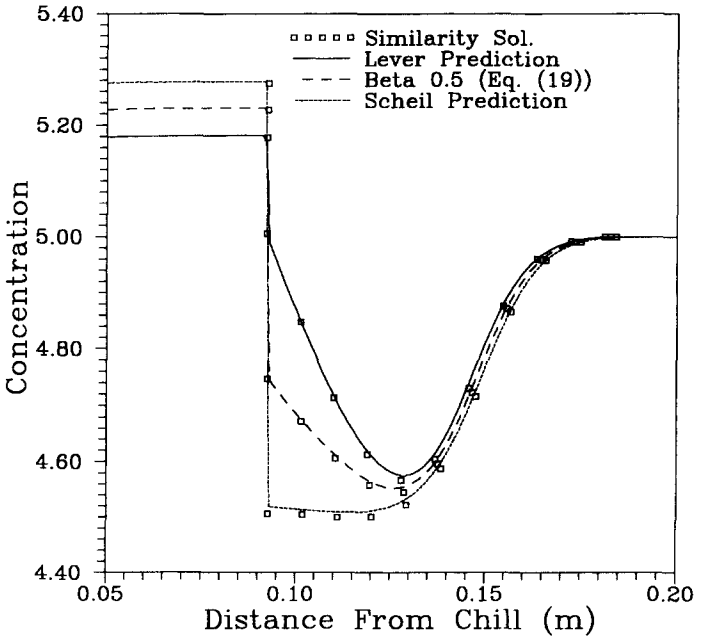

Fig. 4. Concentration profiles at $t = 500$ s predicted with different levels of back-diffusion.

diffusion is presented are in very close agreement with the similarity solution [24].

Figure 5 compares the performance of the Wang and Beckermann [19] back-diffusion model, equation (21) ($\gamma = 0.005$), with the Clyne and Kurz [21] model, equation (19) ($\beta = 0.5$). In the mushy region the predicted concentration profiles, at time $t = 500$ s, indicate that, for finite levels of back-diffusion, the qualitative behavior of the two models is very similar. It is noted, however, that the predicted macrosegregation in the solid phase is different in nature. The use of equation (19) predicts a constant macrosegregation field in the solid whereas the macrosegregation predicted when equation (23) is used shows a gradual decrease as the eutectic front moves away from the chill.

5.4. *Ternary eutectic*

The last set of results presented is for the performance of the proposed scheme in dealing with the

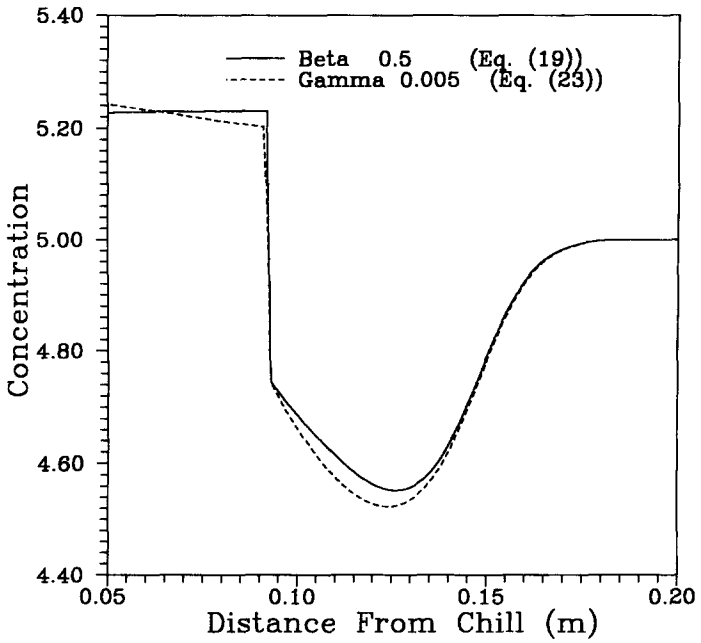

Fig. 5. Concentration profiles at $t = 500$ s predicted with the Clyne and Kurz [23] back-diffusion model and the Wang and Beckermann [19] model.

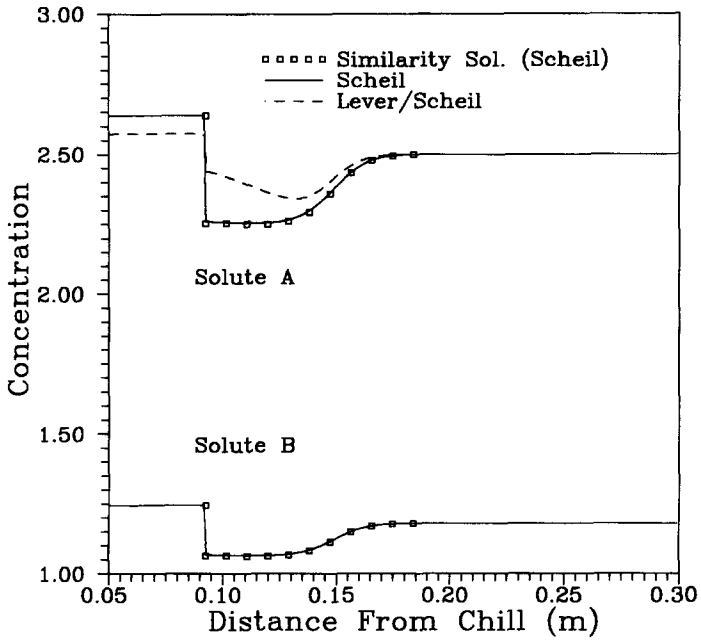

Fig. 6. Concentration profiles at $t = 500$ s in the ternary system.

ternary eutectic system illustrated in Fig. 1. Figure 6 shows the predictions for the concentration profiles in the mushy region for each of the two constituent species at time $t = 500$ s. These predictions assume no solute diffusion at the local scale (the Scheil assumption). As in the case of the binary eutectic system the agreement with the similarity solution is very close. With the current convergence settings the numerical solution of the ternary system needed an average of 5 iterations per time step, a value which is consistent with the performance achieved with computations for a binary alloy.

The numerical model can readily handle problems beyond the scope of the similarity solution. For example the important case where there is a marked difference in the back diffusion behavior between the two constituent species. Shown as a dashed line in Fig. 6 is the numerical prediction of the mixture con-

centrations when solute A has complete back-diffusion and solute B has zero back-diffusion. It is noted that the shape of the concentration profile in solute A lies between those predicted with the lever and Scheil models.

6. CONCLUSIONS

The principal aim of this paper has been to develop a new temperature–solute coupling scheme which is robust, accurate and general. There are four key features in the resulting general scheme:

(1) The use of mixed explicit/implicit time integration.
(2) The use of a simple a simple approximate expression for the liquid fraction temperature slope, dg/dT, used in the linearization of the discrete energy equation, see equation (31).
(3) The ability to easily deal with general local scale behavior, in particular finite diffusion in the solid phase of the REV, see equation (19) or (21).
(4) The ability to easily deal with multicomponent problems.

The first two of these features allows for an efficient and relatively straightforward treatment of a given solidification problem. The last two features allow for the application to a wide range of problems. The performance results presented clearly illustrates these features; indicating that the proposed scheme performs accurately and efficiently across a range of general problems. Of particular note is the very close agreement between the numerical predictions and those obtained with a semi-analytical similarity solution [24]. Current work is directed at establishing a more comprehensive comparison with the similarity solution, e.g. comparisons of temperature and liquid fraction fields predictions [25].

Acknowledgements—The authors acknowledge the support of the Minnesota SuperComputer Institute.

REFERENCES

1. Bennon, W. D. and Incropera, F. P., A continuum model for momentum heat and species transport in binary solid–liquid phase change system—I. Model formulation. *International Journal of Heat and Mass Transfer*, 1987, **30,** 2161–2170.
2. Bennon, W. D. and Incropera, F. P., A continuum model for momentum heat and species transport in binary solid–liquid phase change system—II. Application to solidification in a rectangular cavity. *International Journal of Heat and Mass Transfer*, 1987, **30,** 2171–2187.
3. Bennon, W. D. and Incropera, F. P., The evolution of macrosegregation in statically cast binary ingots. *Metallurgical Transactions B*, 1987, **18,** 611–612.
4. Bennon, W. D. and Incropera, F. P., Numerical analysis of binary solid–liquid phase change using a continuum model. *Numerical Heat Transfer*, 1988, **13,** 277–296.
5. Beckermann, C. and Viskanta, R., Double-diffusive convection during dendritic solidification of a binary mixture. *Physics Chemistry Hydrology*, 1988, **10,** 195–213.
6. Voller, V. R., Brent, A. D. and Prakash, C., The modeling of heat, mass and solute transport in solidification systems. *International Journal of Heat and Mass Transfer*, 1989, **32,** 1719–1731.
7. Prakash, C. and Voller, V. R., On the numerical solution of continuum mixture model equations describing solid–liquid phase change. *Numerical Heat Transfer B*, 1989, **15,** 171–189.
8. Flood, S. C., Kattgerman, L. and Voller, V. R., The calculation of heat and fluid flows in the D.C. casting of aluminum alloys, modeling of casting. *Welding and Advanced Solidification Processes, V*. TMS-AIME, Warrendale, PA. 1991.
9. Rappaz, M. and Voller, V. R., Modeling micro-macrosegregation in solidification processes. *Metallurgical Transactions A*, 1990, **21,** 749–753.
10. Voller, V. R. and Sundarraj, S., A model of inverse segregation: the role of microporosity. *International Journal of Heat and Mass Transfer*, 1995, **38,** 1009–1018.
11. Nandapurkar, P., Poirier, D. R., Heinrich, J. C. and Felicelli, S., Thermosolutal convection during dendritic solidification of alloys: part I. Linear stability analysis. *Metallurgical Transactions B*, 1989, **20,** 711–721.
12. Nandapurkar, P., Poirier, D. R., Heinrich, J. C. and Felicelli, S., Thermosolutal convection during dendritic solidification of alloys: part II. Nonlinear convection. *Metallurgical Transactions B*, 1989, **20,** 883–891.
13. Diao, Q. Z. and Tsai, H. L., Modeling of solute redistribution in the mushy zone during solidification of aluminum–copper alloys. *Metallurgical Transactions A*, 1993, **24,** 963–973.
14. Chen, J. H. and Tsai, H. L., Inverse segregation for a unidirectional solidification of Al–Cu alloys. *International Journal of Heat and Mass Transfer*, 1993, **36,** 3069–3075.
15. Zeng, Xin and Faghri, Amir, Temperature-transforming model for binary solid–liquid phase-change problems part I: mathematical modeling and numerical methodology. *Numerical Heat Transfer B*, 1994, **25,** 467–480.
16. Zeng, Xin and Faghri, Amir, Temperature-transforming model for binary solid–liquid phase-change problems part II: numerical solution. *Numerical Heat Transfer B*, 1994, **25,** 481–500.
17. Schneider, M. C. and Beckermann, C., Formation of macrosegregation by multicomponent thermosolutal convection during the solidification of steel. *Metallurgical Transactions A*, 1995, **26,** 2373–2388.
18. Ni, J. and Beckermann, C., A volume-averaged two-phase model for transport phenomena during solidification. *Metallurgical Transactions B*, 1991, **22,** 349–361.
19. Wang, C. Y. and Beckermann, C., A multiphase solute diffusion model for dendritic solidification. *Metallurgical Transactions A*, 1993, **24,** 2787–2802.
20. Poirier, D. R. and Nandapurkar, P., Enthalpies of a binary alloy during solidification. *Metallurgical Transactions A*, 1988, **19,** 3057–3061.
21. Clyne, T. W. and Kurz, W., Solute redistribution during solidification with rapid state diffusion. *Metallurgical Transactions A*, 1981, **12,** 965–971.
22. Brody, H. B. and Flemings, M. C., Solute redistribution in dendritic solidification. *Transactions AIME*, 1996, **236,** 615–624.
23. Swaminathan, C. R. and Voller, V. R., On the enthalpy method. *International Journal of Heat and Fluid Flow*, 1993, **3,** 233–234.
24. Voller, V. R., A similarity solution for the solidification of a multicomponent alloy. *International Journal of Heat and Mass Transfer*, 1997, **40,** 2869–2877.
25. Voller, V. R., A numerical scheme for solidification of an alloy. *Canadian Metallurgical Quarterly*, 1996 (submitted).